Nonlinear Schrödinger invariants and nonlinear wave statistics

F. Fedele,[1,a)] Z. Cherneva,[2,b)] M. A. Tayfun,[3,c)] and C. Guedes Soares[2,d)]
[1]*School of Civil and Environmental Engineering, Georgia Institute of Technology, Savannah, Georgia 31407, USA*
[2]*Centre for Marine Technology and Engineering (CENTEC), Technical University of Lisbon, Instituto Superior Técnico, Lisbon 1049-001, Portugal*
[3]*Department of Civil Engineering, Kuwait University, Safat 13060, Kuwait*

(Received 16 September 2009; accepted 26 January 2010; published online xx xx xxxx)

AQ: #2

Third-order quasiresonant interactions among free waves and associated modulational instabilities can significantly affect the statistics of various surface features in narrowband waves. In particular, modulational instabilities tend to induce intermittent amplifications on the surface displacements, causing their statistics to deviate from the linear Gaussian and second-order models. Herein, we investigate the nature of such instabilities on the statistical and spectral characteristics of deep-water waves generated in a large wave basin. We analyze the spectral changes that occur as waves propagate along the basin, develop bounds on the spectrum bandwidth, and interpret various statistics based on third-order Gram–Charlier distributions.
[doi:10.1063/1.3325585]

I. INTRODUCTION

Surface waves are nonlinear in nature, in particular, relatively long-crested waves because of their tendency to be affected by the interactions among freely propagating elementary waves with random amplitudes and phases. Consequently, their dynamics, kinematics, and spectral evolution in space and time are often interpreted stochastically, using perturbation models. If nonlinearities are not particularly significant, the statistics of various surface features tend to follow a Gaussian structure, modeled as the linear superposition of a large number of elementary wavelets with Rayleigh-distributed amplitudes and random phases. At this level of approximation, surface displacements are "symmetric" with respect to the mean sea level. As a result, wave crest and trough amplitudes are Rayleigh-distributed, and large waves are likely to be generated by the linear focusing of elementary phases (Lindgren,[1] Boccotti,[2,3] Fedele,[4] and Fedele and Tayfun[5]).

At the next level of approximation to $O(\varepsilon)$ in wave steepness ε, the perturbations of the Stokes equations lead to a variety of random models in which the first-order Gaussian structure is modified by second-order nonresonant bound waves (see, e.g., Longuet-Higgins[6]). The latter are non-Gaussian and phase-coupled to the linear waves, making wave crests sharper and narrower and troughs shallower and more rounded. As a result, surface elevations are positively skewed, and the distributions of wave crests and trough amplitudes asymmetrically deviate from the Rayleigh law (Fedele and Tayfun[5]). Models constructed to reflect such second-order nonlinearities tend to describe the statistics of wave heights, and crest and trough amplitudes fairly accurately (Fedele and Tayfun,[5] Tayfun and Fedele,[7] and Tayfun[8]).

To $O(\varepsilon^2)$, third-order multiple scale perturbation solutions of the Stokes equations show that energy is transferred via resonant and quasiresonant interactions to longer and also shorter scales where it is dissipated by breaking or viscous dissipation. The resulting sea state is referred to as "wave" or "weak" turbulence (WT) in analogy with the Kolmogorov energy cascade in fluid turbulence (Zakharov[9,10]). WT states ensue from the space-time evolution of a sea of weakly nonlinear coupled dispersive waves in accordance with the Zakharov equation,[9] valid for an arbitrary spectral width. In WT, an initial Gaussian field is weakly modulated as nonlinearities develop in time, leading to intermittency in the turbulent signal due to the formation of sparse but coherent structures. In recent numerical studies (see, e.g., Onorato *et al.*[11]), it is speculated that the large wave crests observed during these localized events may explain the occurrence of abnormal, rogue or freak waves. These are unusually large waves that appear from nowhere in the open ocean, as has been identified in records of full scale waves (Guedes Soares *et al.*[12,13]). Their frequency of occurrence significantly exceeds the theoretical predictions based on linear Gaussian or second-order statistical models (Socquet-Juglard *et al.*,[14] Petrova *et al.*,[15] and Dysthe *et al.*[16]).

Up to date, rogue waves have systematically been observed in unidirectional narrowband waves mechanically generated in tanks (Onorato *et al.*,[17,18] Petrova and Guedes Soares,[19] Shemer and Sergeeva,[20] and Cherneva *et al.*[21]). Near-resonant interactions and associated Benjamin–Feir-type modulational instabilities[22] appear as the essential features of the evolutionary dynamics of such waves. Typically, an initially narrowband wave train can undergo intense modulations, attended by an asymmetrical growth of the spectral sidebands, enhancing the occurrence of larger waves (Janssen[23]). As a result, the distribution of wave and crest

[a)]Electronic mail: francesco.fedele@gtsav.gatech.edu.
[b)]Electronic mail: cherneva@mar.ist.utl.pt.
[c)]Elelctronic mail: aziztayfun@usa.net.
[d)]Electronic mail: guedess@mar.ist.utl.pt.

heights can deviate from the linear and second-order models. This is confirmed by the numerical simulations of Dysthe's modified nonlinear Schrödinger (MNLS) equation (Dysthe,[24] Socquet-Juglard *et al.*,[14] and Dysthe *et al.*[16]).

In a recent study, Shemer and Sergeeva[20] described the evolution of narrowband nonlinear waves in a large wave channel. Unidirectional waves generated at the wave maker from an initially narrowband Gaussian-shaped spectrum were subsequently measured at numerous locations as they propagated along the channel. The statistics of the unusually large wave heights, and crest and trough amplitudes observed in these experiments are explained reasonably well by theoretical approximations based on Gram–Charlier (GC) expansions (Tayfun and Fedele[7]). In essence, such approximations represent Hermite series expansions of distributions describing non-Gaussian random functions (Longuet-Higgins[6]). They are related to the stochastic structure of waves only through certain key statistics such as the skewness and kurtosis of surface displacements whose closed-form solutions in terms of surface spectra follow from Zakharov's WT model (see, e.g., Fedele[4]).

In this study, we will analyze nonlinear waves generated in a large wave basin at Marintek, Trondheim, Norway in 1999. The surface elevations measured at several gauges placed along the basin display relatively strong nonlinearities and contain an adequately large population of freak waves for reliable statistical analyses and comparisons with the theoretical models. In particular, we focus attention only on the effects of quasiresonant interactions on various statistics observed during the experiments. In order to interpret the statistics, we draw on the spatial version of the nonlinear Schrödinger (NLS) equation. Shemer *et al.*[25] show that Dysthe's MNLS is more accurate than the NLS model for describing the evolution of groups of strongly nonlinear waves generated in wave tanks. Nonetheless, the NLS model and its properties have not been fully explored in interpreting the spectral and statistical characteristics of random waves of moderate steepness, in particular, directly from experimental time series. Here, we attempt to do so. Our work reveals that although the NLS model cannot model various nonlinearities such as the $O(\varepsilon)$ front-rear asymmetry of wave groups and dispersion effects as higher order models do, it does nonetheless describe the surface statistics fairly well. Further, we exploit the integrals of motion to analyze how the surface spectra change spatially along the wave basin, establish bounds on the spectrum bandwidth, and derive an analytical expression describing the spatial variation of the excess kurtosis of surface displacements. Finally, we construct the empirical distributions describing wave heights, crest and trough amplitudes observed, and compare these with the GC distributions proposed by Tayfun and Fedele.[7]

II. NLS MODEL

We consider the spatial NLS equation valid for narrowband waves in deep water (Mei[26]). To $O(\varepsilon^2)$, the surface displacement η from the mean water level, observed at a fixed point x in time t, can be expressed as

$$\eta(x,t) = \mathrm{Re}\left\{ a_0 B \exp(i\phi) + \frac{k_m a_0^2 B^2}{2}\exp(2i\phi) + \frac{3k_m^2 a_0^3 B^3}{8}\exp(3i\phi)\right\}, \qquad (1)$$

where $\mathrm{Re}\{z\}$ denotes the real part of z, $B(\xi,\tau)$ is the complex envelope, $\phi = k_m x - \omega_m t + \theta$, θ is the wave phase uniformly distributed in $(0,2\pi)$ initially at $x=0$, $\varepsilon = a_0 k_m$ is the wave steepness, a_0 is the characteristic amplitude, c_g is the group velocity corresponding to the spectral "mean" frequency ω_m, and wave number such that $k_m = \omega_m^2/g$. The complex envelope satisfies the damped version of the NLS equation[26]

$$\partial_\xi B + i\partial_\tau^2 B + i|B|^2 B = -\gamma B, \qquad (2)$$

where

$$\tau = \varepsilon\omega_m\left(t - \frac{x}{c_g}\right), \quad \xi = \varepsilon^2 k_m x.$$

For a rectangular wave flume of width b, the viscous damping coefficient γ can be expressed as (Kit and Shemer[27] and Shemer *et al.*[28])

$$\gamma = \frac{2k_m}{b}\sqrt{\frac{\nu_e}{\omega_m}}\exp(-i\pi/4), \qquad (3)$$

where ν_e represents an effective viscosity coefficient.

The complex envelope can be expressed in the form $a_0 B = \eta_1 + i\hat{\eta}_1$ where the linear component η_1 of the surface displacement and its Hilbert transform $\hat{\eta}_1$ are given by

$$\eta_1 = a_0|B|\cos(\vartheta + \phi), \quad \hat{\eta}_1 = a_0|B|\sin(\vartheta + \phi), \qquad (4)$$

where

$$|B| = (\eta_1^2 + \hat{\eta}_1^2)^{1/2}/a_0, \quad \vartheta = \tan^{-1}(\hat{\eta}_1/\eta_1) - \phi.$$

As a result, the surface displacement (1) can be rewritten as

$$\eta = \eta_1 + \eta_2 + \eta_3, \qquad (5)$$

with

$$\eta_2 = \frac{k_m}{2}(\eta_1^2 - \hat{\eta}_1^2), \quad \eta_3 = \frac{3k_m^2}{8}(\eta_1^3 - 3\eta_1\hat{\eta}_1^2). \qquad (6)$$

Hereafter, we set $a_0 = \max(\eta_1)$, and also let S_{η_1} and S_η denote the frequency spectra of η_1 and η, respectively. The ordinary moments of S_{η_1} are m_j $(j=0,1,2,\ldots)$ so that $\sigma^2 = m_0 \equiv$ variance of η_1, $\omega_m = m_1/m_0$, and $\nu = (m_0 m_2/m_1^2 - 1)^{1/2} \equiv$ spectral bandwidth. Also, because the statistics of η has previously been investigated elsewhere (Onorato *et al.*,[17,18] Shemer and Sergeeva,[20] and Cherneva *et al.*[21]), we will focus on η_1 and its statistics as affected by quasiresonant interactions and associated modulational instabilities. To do so based on an observational time series of η, the second- and third-order bound harmonics will have to be removed. Here, we follow a procedure similar to that described by Tayfun[8] and solve Eq. (1) for η_1 via inversion and then require $\langle\eta_1^3\rangle = 0$ (see Appendix A). To convey a physical picture of what ensues from this procedure, we show in Fig. 1 a partial time series of η measured at one of the gauges at Marintek,

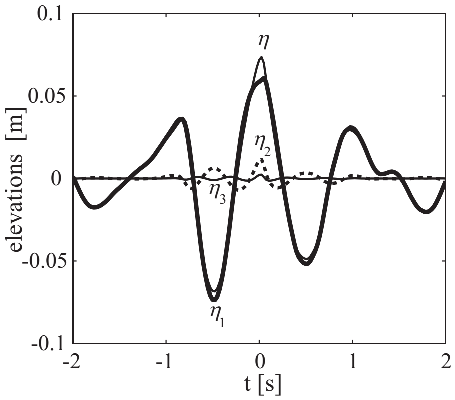

FIG. 1. A segment of the full surface elevation η observed at $x=45$ m (gauge 8), the corresponding free wave η_1, and the second and third-order corrections (η_2 and η_3) removed from η to obtain η_1.

the second- and third-order bound harmonics removed from it, and the resulting free-wave profile η_1.

III. NLS properties of η_1

Consider the wave action, momentum and Hamiltonian defined, respectively, by (cf. Ablowitz and Segur[29])

$$\mathbf{A} = \langle |B|^2 \rangle,$$

$$\mathbf{M} = i\langle B\partial_\tau B^* - B^*\partial_\tau B\rangle/2,$$

$$\mathbf{H} = \langle |\partial_\tau B|^2 - |B|^4/2\rangle, \tag{7}$$

where the angle brackets represent averages with respect to τ. If viscous damping is excluded from Eq. (3) by setting $\gamma=0$, the preceding expressions will represent the integrals of motion which do not depend on the spatial coordinate ξ. However, in the most general case, they do vary with ξ along the experimental basin because of wave breaking and/or viscous dissipation of high-frequency spectral components not described by the NLS equation. To describe the spectral variability of waves, we define a convenient measure for the bandwidth of S_{η_1} as

$$\Delta_\omega^2 = \varepsilon^2 \frac{\langle |\partial_\tau B|^2\rangle}{\langle |B|^2\rangle}. \tag{8}$$

Using the exponential form of B and Eq. (2), the preceding definition can be rewritten as

$$\Delta_\omega^2 = \varepsilon^2 \frac{\langle |B|^2 \Delta\omega^2 + (\partial_\tau |B|)^2\rangle}{\langle |B|^2\rangle}. \tag{9}$$

Physically, $\Delta\omega = \partial_\tau \vartheta$ represents a relative measure for the dispersion or spread of spectral frequencies around ω_m, and so does Δ_ω. In the NLS theory, Δ_ω is not an invariant since it can vary with ξ. Defining Δ_ω has the advantage that it is easily estimated directly from a time series, whereas the conventional bandwidth measure ν requires the spectral moments of η_1. Also, the analysis of the Marintek data will show later on that Δ_ω and ν are practically the same. Perhaps, more significantly, the NLS theory allows us to derive certain spatially uniform upper and lower bounds for Δ_ω which are invariants as those in Eq. (7) if viscous dissipation is neglected. To do so, we use Eq. (7) and write Eq. (8) as

$$\Delta_\omega^2 = \varepsilon^2 \left(\frac{\mathbf{H}}{\mathbf{A}} + \frac{\langle |B|^4\rangle}{2\langle |B|^2\rangle} \right). \tag{10}$$

It readily follows then that given ξ,

$$\Delta_L \le \Delta_\omega \le \Delta_U, \tag{11}$$

where

$$\Delta_L = \varepsilon \sqrt{\frac{\mathbf{H}}{\mathbf{A}}}, \quad \Delta_U = \frac{\varepsilon}{2}\mathbf{A}\left[1 + \sqrt{1 + \frac{4}{\mathbf{A}^2}\left(\frac{\mathbf{H}}{\mathbf{A}} + \frac{\mathbf{A}}{2}\right)} \right]. \tag{12}$$

In general, these bounds are not sharp, but spatially invariant. Indeed, Δ_L holds only when $\mathbf{H} \ge 0$ and follows directly from Eq. (10) by neglecting the non-negative spatially varying term between parentheses (the term $\mathbf{H}/\mathbf{A}$ is the only invariant), whereas Δ_U was derived by Thyagaraja[30] and it is valid for any $\mathbf{H}$.

The surface spectrum can vary with ξ as waves propagate along the wave basin, but it is not expected to violate the bounds in Eq. (12) and as $\xi \to \infty$ it asymptotically relaxes toward a statistically stationary state. This is what is observed in both numerical simulations and experiments (Socquet-Juglard *et al.*[14] Shemer and Sergeeva[20]).

IV. MARINTEK EXPERIMENTS

Marintek data were obtained during a sequence of five experiments run in a wave basin 80 m long and 50 m wide. Surface displacements were measured by ten capacitance wave gauges placed along the centerline of the basin. The first gauge is at 10 m from a double-flap wave maker, and the subsequent ones are placed at a uniform spacing of 5 m along the section where the water depth is 2 m. The spectrum generated at the wave maker is of the JONSWAP type with the Phillips parameter 0.0178, a peak-enhancement factor of 3, peak frequency $\omega_p = 6.343$ rad s^{-1}, and it is bandlimited to frequencies in $(0, 3\omega_p)$. For waves generated at the wave maker, $\nu = 0.298$, $k_p = \omega_p^2/g = 4.105$ m^{-1} and steepness $\sigma k_p = 0.072$ so that principal wave components such as those associated with the peak and mean frequencies are essentially in deep water. A more detailed description of these experiments is given by Cherneva *et al.*[21]

From a time series of η measured at a gauge, we first estimate the free-wave component η_1 via inversion, as described in Appendix A. Table I summarizes the ensemble average values of σ, ν, ω_m and k_m for η_1 obtained from the five experimental series of η at gauges 1–10, where x denotes the distance from the maker. They are similar in nature to those of η actually observed (see Cherneva *et al.*,[21] Table I). In either case, because some waves simulated in these experiments are rather small and high-frequency, they are prone to viscous damping as they propagate along the relatively long wave basin. This explains at least partially why the parameters listed in Table I here and also in the work of Cherneva *et al.*[21] tend to decrease steadily with distance from the wave maker.

AQ: #8

TABLE I. η_1: principal spectral parameters.

x (m)	σ (m)	ω_m (s^{-1})	k_m (m^{-1})	ν
10	0.019	7.108	5.150	0.267
15	0.018	7.023	5.028	0.261
20	0.018	6.954	4.930	0.257
25	0.017	6.940	4.910	0.253
30	0.017	6.910	4.867	0.256
35	0.016	6.868	4.808	0.257
40	0.016	6.832	4.759	0.247
45	0.016	6.805	4.721	0.249
50	0.016	6.775	4.679	0.246
55	0.016	6.761	4.660	0.241

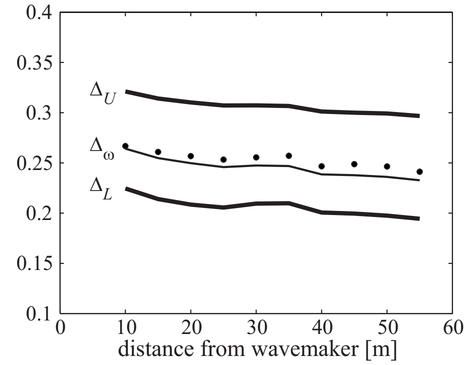

FIG. 3. Free wave η_1: the spatial variations of Δ_ω, its lower and upper bounds and ν (points), all representing the average values of five experiments.

The envelope B observed at each wave gauge is constructed from Eq. (3), using the values $a_0=0.074$ m and $\omega_m=7.108$ rad s^{-1} observed at gauge 1. This approach enables us to obtain from Eq. (7), the spatial variations of $\mathbf{A}$, $\mathbf{M}$, and $\mathbf{H}$, shown in Fig. 2. Evidently, all three averages tend to decrease somewhat with distance from the wave maker as waves propagate along the basin, plausibly due to the various dissipative effects previously mentioned. If we consider the damped NLS model (2), then the spatial damping of wave action $\mathbf{A}$ is described by $d\mathbf{A}/d\xi=-2\gamma_r\mathbf{A}$, where $\gamma_r = k_m\sqrt{2\nu_e/\omega_m}/b$ and follows from the real part of Eq. (6). Thus, $\mathbf{A}(\xi)=\mathbf{A}(0)\exp(-2\gamma_r\xi)$, where γ_r and thus ν_e are easily estimated from the observed values of $\mathbf{A}$ by regression analysis. This process leads us in the present case to the estimates $\gamma_r \cong 3.4\times 10^{-3}$ m^{-1} and $\nu_e \cong 1.5\times 10^{-3}$ m^2 s^{-1}.

As viscous effects dissipate relatively miniscule high-frequency waves as they propagate along the basin, the spectrum bandwidth ν also gradually decreases, as shown in Table I. Figure 3 shows how Δ_ω and the associated lower and upper bounds vary at different gauges along the channel. The variation of ν is also included in the same figure which suggests that it is practically the same as Δ_ω. Clearly, Δ_ω does decrease along the basin as ν does, but it does not violate the theoretical bounds in Eq. (11). This is confirmed in Fig. 4 more explicitly by the gradual damping of relatively high-frequency components in the ensemble-averaged spectra S_η and S_{η_1} at increasing distances $x=10$, 35, and 45 m from the wave maker, respectively. A slight downshifting of the spectral peak is also noticeable in this figure, plausibly due to quasiresonant modulations. One would also expect to see a widening of the spectra for the same reason, as in the experiments of Shemer and Sergeeva[20] with larger waves characterized by more intense modulations than here. In contrast, Figs. 3 and 4 both clearly show that this does not really happen in this particular set of experiments, again possibly because of the viscous damping of high-frequency components. Evidently, spectral slopes tend to behave as ω^{-5} closer to the wave maker, and eventually steepen to approximate a ω^{-6} viscous range. The gradual downshift of the mean frequency ω_m of η_1 with distance along the basin, as seen in Table I here and similarly for η (see Cherneva *et al.*,[21] Table

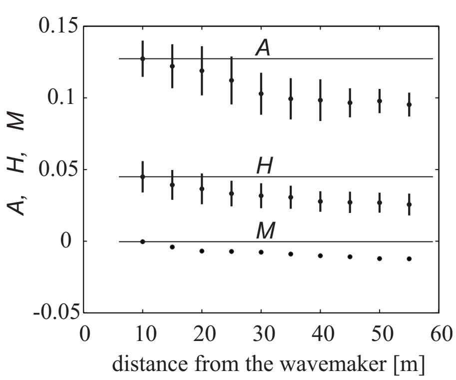

FIG. 2. Spatial variations of the averaged Hamiltonian $\mathbf{H}$, wave action $\mathbf{A}$ and momentum $\mathbf{M}$. Each point represents an overall average of five experimental series with the range of values observed in separate series indicated by vertical lines (not clearly visible for $\mathbf{M}$). The horizontal straight lines correspond to the expected theoretical values along the channel in accord to the NLS model.

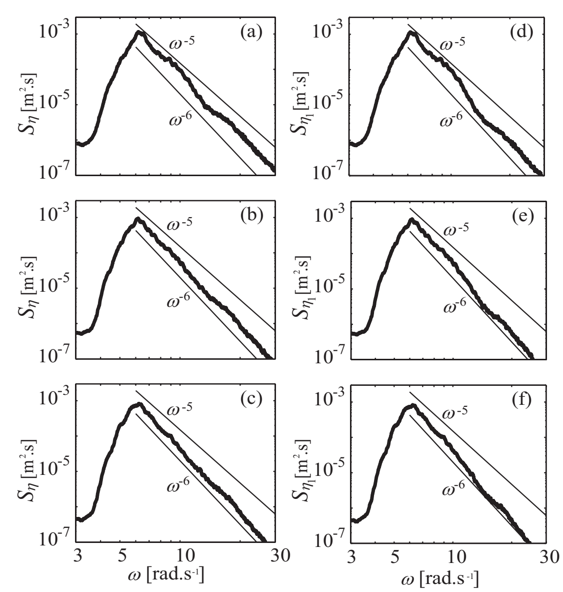

FIG. 4. Average spectra S_η of the actual series η observed at (a) $x=10$ m (gauge 1), (b) $x=30$ m (gauge 5), and (c) $x=45$ m (gauge 8) from the wave maker. Similarly, the spectra S_{η_1} of the corresponding free-wave series η_1 observed at (d) $x=10$ m, (e) $x=30$ m, and (f) $x=45$ m from the wave maker.

I), is consistent with this interpretation. Other experiments carried out at Marintek more recently also report quite similar results (see, e.g., Onorato *et al.*[18]).

V. EXCESS KURTOSIS OF η_1

Closer to the wave maker, free-wave component η_1 is quasi-Gaussian. As waves propagate away from the wave maker, nonlinear interactions gradually build up, leading to intermittency. Larger waves occur more frequently and the surface statistics tend to deviate from the linear Gaussian models. The natural presence of second- and third-order nonresonant bound interactions in the fully nonlinear surface displacement η amplifies these further. In particular, previous investigations by Onorato *et al.*,[17,18] Shemer and Sergeeva,[20] Cherneva *et al.*,[21] Petrova *et al.*,[31] and others suggest that the frequency of occurrence of unusually large waves increases noticeably, accompanied by an increase in the excess kurtosis λ_{40} of η. These results reflect the combined effects of resonant and nonresonant interactions as they are coupled through Eq. (1).

Here, we focus on the excess kurtosis λ_{40} of η_1 and explore the effects of quasiresonant interactions only. In this context, Mori and Janssen[32] have previously derived an analytical expression describing λ_{40} during the temporal evolution of spatially homogenous waves. In the present case, we consider the spatial evolution of stationary waves based on the spatial NLS equation (4), which is more appropriate for waves simulated in tanks. The spatial variation of λ_{40} of η_1 follows with relative ease from the stochastic formulation of nonlinear wave groups, elaborated by Fedele[8] for the Zakharov equation.[9] Using the latter formulation coupled with the general theory of quasideterminism of Boccotti,[2,3] Fedele[8] derived an expansion of the highest nonlinear crest in terms of Rayleigh-distributed variables from the Zakharov equation directly. A comparison of coefficients in that expansion to those in the GC-type crest models (Tayfun and Fedele[7]) leads to an analytical expression for λ_{40} in terms of S_{η_1}. This expression is identical to the result obtained by Janssen[23] and Mori and Janssen.[32] For the NLS model of Eq. (2) with $\gamma=0$, it assumes the form

$$\lambda_{40} = 24(k_m\sigma)^2 \int\int\int S_{\eta_1}(w_1)S_{\eta_1}(w_2)S_{\eta_1}(w_3)\frac{1-\cos(Wk_m x)}{W\sigma^6}dw_1dw_2dw_3, \tag{13}$$

where $W=w^2+w_1^2-w_2^2-w_3^2$, $w=-w_1+w_2+w_3$, and $w_j=(\omega_j/\omega_m-1)$ for $j=1$, 2, and 3, S_{η_1} represents the initial spectrum at the wave maker where $x=0$, and the limits of integration are from $-\infty$ to ∞. For a Gaussian-shaped initial spectrum

$$S_{\eta_1}(\omega) = \frac{\sigma^2}{\sqrt{2\pi\nu^2}}\exp\left(-\frac{(\omega/\omega_m-1)^2}{2\nu^2}\right), \tag{14}$$

Eq. (13) is simplified to

$$\lambda_{40}(x) = 12(k_m\sigma/\nu)^2 J(\alpha), \tag{15}$$

where $\alpha=2\nu^2k_mx$ and

$$J(\alpha) = \frac{1}{(2\pi)^{3/2}} \times\int\int\int \exp\left(-\frac{z_1^2+z_2^2+z_3^2}{2}\right)\frac{1-\cos Z}{Z}dz_1dz_2dz_3. \tag{16}$$

In the preceding expressions, $Z=(z_1-z_3)(z_2-z_3)$, x is the distance of a wave gauge from the wave maker, and k_m, σ, and ν are the initial values at the wave maker. Carrying out the integration in Eq. (16) leads to (see Appendix B)

$$\lambda_{40}(x) = 4\sqrt{3}\left(\frac{k_m\sigma}{\nu}\right)^2\left\{\frac{\pi}{6} - \mathrm{Im}\left[i\sin^{-1}\left(\frac{1+2i\alpha}{2}\right)\right]\right\}, \tag{17}$$

where Im$\{z\}$ denotes the imaginary part of z. As $\alpha\to\infty$, $J(\infty)\to\pi/6\sqrt{3}$, which agrees with the result obtained by Mori and Janssen.[32] Thus, at steady state, λ_{40} is the same for both the spatial and temporal cases, as it should be when waves become statistically homogenous. Figure 5 compares Eq. (17) to the Marintek data. The observed values of λ_{40} compare fairly well with the theoretical predictions sufficiently away from the wave maker where free-wave interac-

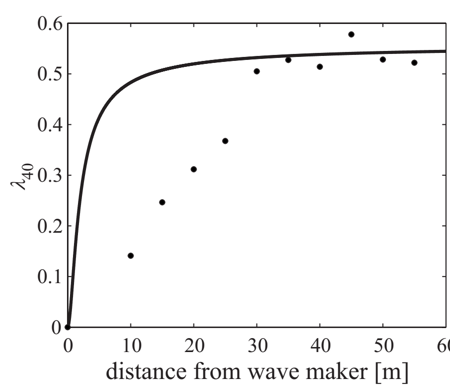

FIG. 5. Excess of kurtosis λ_{40} of η_1 (points) compared with the NLS theory from Eq. (17) (continuous curve) based on $k_m\sigma=0.093$ and $\lambda=0.267$ at the wave maker.

AQ: #9

TABLE II. η_1: nontrivial cumulants λ_{mn}, Λ and Λ_{app}/Λ.

x (m)	λ_{40}	λ_{22}	λ_{04}	Λ	Λ_{app}/Λ
10	0.141	0.047	0.144	0.380	0.986
15	0.246	0.080	0.235	0.643	1.027
20	0.312	0.099	0.283	0.793	1.050
25	0.367	0.121	0.360	0.970	1.011
30	0.505	0.163	0.476	1.307	1.031
35	0.528	0.177	0.533	1.415	0.995
40	0.514	0.170	0.506	1.360	1.008
45	0.578	0.191	0.566	1.526	1.010
50	0.528	0.172	0.504	1.377	1.025
55	0.522	0.172	0.513	1.380	1.012

tions become significant. This agrees with the recent simulations of the Zakharov model by Annenkov and Shrira,[33] clearly showing that kurtosis in narrowband waves is mostly due to nonlinear quasiresonant interactions whereas it is almost entirely due to bound harmonics in broadband wind waves.

VI. THEORETICAL DISTRIBUTIONS

Tayfun and Fedele[7] describe various GC distributions for approximating the statistics of nonlinear random waves. These can be used for describing the statistics of η_1 just as well as the fully nonlinear η. Various results relevant to the statistics of η can be found in previous studies (Tayfun and Fedele,[7] Tayfun,[8] Shemer and Sergeeva,[20] and Cherneva *et al.*[21]). Here, we consider the statistics of η_1 for which the steepness parameter defined by $\mu = \langle \eta_1^3 \rangle / 3$, one of two key parameters in the GC-type distributions, is zero since η_1 is derived from η so that $\langle \eta_1^3 \rangle = 0$. On this basis, the GC exceedance distribution describing the crest and trough amplitudes of η_1 easily follows, by setting $\mu = 0$ in the expressions of Tayfun and Fedele,[7] as

$$Q_{GC}^{\pm}(z) \equiv \Pr\{\varsigma > z\} = \exp\left(-\frac{z^2}{2}\right)\left[1 + \frac{\Lambda}{64} z^2 (z^2 - 4)\right], \tag{18}$$

where ς stands for the wave crest or trough amplitude scaled with σ and

$$\Lambda \equiv \lambda_{40} + 2\lambda_{22} + \lambda_{04}, \tag{19}$$

for simplicity, with $\lambda_{40} \equiv \langle \eta_1^4 \rangle - 3$, $\lambda_{22} \equiv \langle \eta_1^2 \hat{\eta}_1^2 \rangle - 1$, and $\lambda_{04} \equiv \langle \hat{\eta}_1^4 \rangle - 3$. Evidently, η_1 is non-Gaussian, but its crest and trough amplitudes have the same distribution (18). The symmetric amplifications imposed on them by quasiresonant interactions are reflected in the parameter Λ. In linear waves, $\Lambda \cong 0$ and Eq. (18) reduces to the Rayleigh exceedance distribution given by

$$Q_R(z) = \exp(-z^2/2). \tag{20}$$

The exceedance distribution describing the statistics of large crest-to-trough wave heights scaled with σ, say h, in Gaussian seas are described fairly accurately by the theoretical expressions devised by Boccotti[2,3] and Tayfun.[34] For narrowband waves, $h \approx 2\zeta$ so that both expressions tend to the Rayleigh limit of the form

$$Q_h(z) = \Pr\{h > z\} \approx \exp(-z^2/8). \tag{21}$$

AQ: #2

Although second-order nonlinearities do not appear to affect the statistics of wave heights significantly, third-order quasiresonant interactions and associated modulational instabilities do so. The appropriate GC model accounting for the latter effects on η_1 follows, again by setting $\mu = 0$ in the expressions given by Tayfun and Fedele,[7] as

$$Q_{GC}(z) = Q_h(z)\left[1 + \frac{\Lambda}{1024} z^2 (z^2 - 16)\right]. \tag{22}$$

Table II summarizes the ensemble averaged nontrivial values of the cumulants λ_{nm} of η_1 and the resulting Λ observed at gauges 1–10. All other third and fourth-order cumulants not shown in this table are zero to two decimals. This essentially confirms the relative validity of the procedure we have used in removing the bound harmonics from η to obtain η_1. Further, the fourth-order moments and thus Λ tend to monotonically increase with distance from the wave maker. This tendency is a clear indication of the progressive development of quasiresonant modulations as waves propagate along the basin. Also, notice that for η_1, all values of λ_{nm} and Λ in Table I satisfy the equalities $\lambda_{40} = 3\lambda_{22} = \lambda_{04}$ and $\Lambda_{app} = 8\lambda_{40}/3 = \Lambda$ very nearly, as suggested by Mori and Janssen.[32] As a result, the theoretical expressions which require Λ can be expressed in simpler forms dependent solely on the excess kurtosis λ_{40} of η_1. Unfortunately, however, the same equalities do not generally hold for η (see Cherneva *et al.*,[21] Table II).

VII. COMPARISONS

The comparisons here will focus only on the measurements at gauges 1, 5, and 8, located at $x = 10$, 30, and 45 m from the wave maker, respectively. At these locations, the third-order quasiresonant interactions appear to be at their initial, intermediate and peak stages of development. The distributions of η_1 observed at these gauges will be compared to the predictions from the third-order GC distributions, represented by Eq. (18) for crest and trough amplitudes, and Eq. (22) for wave heights. For contrast, we will

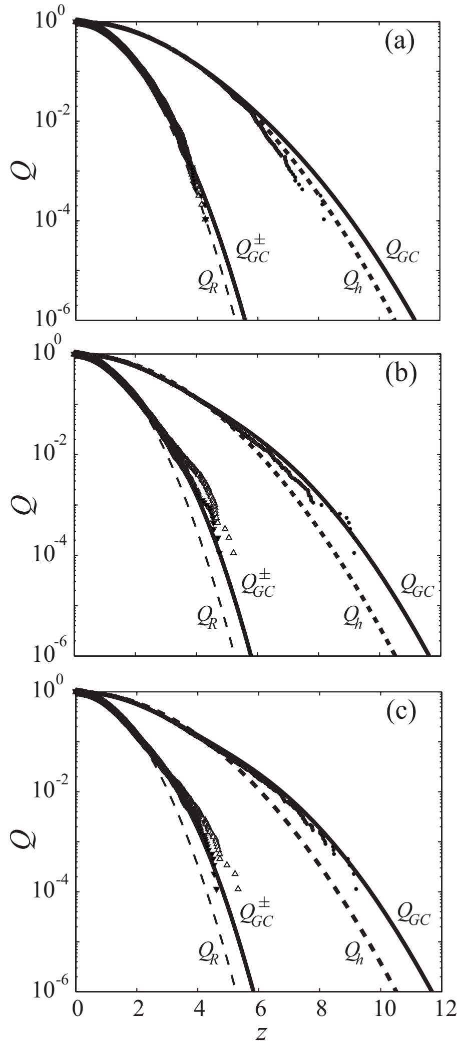

FIG. 6. Exceedance distributions observed at (a) $x=10$ m (gauge 1), (b) $x=30$ m (gauge 5), and (c) $x=45$ m (gauge 8) from the wave maker, describing wave heights (points), crests (hollow triangles) and trough amplitudes (solid triangles) compared with the predictions from $Q_{\mathrm{GC}}^{\pm}$ of Eq. (18) for wave crest and trough amplitudes, and Q_{GC} of Eq. (22) for wave heights. Gaussian limits (dashed curves) are represented by Q_R of Eq. (20) for linear crest and trough amplitudes and Q_h of Eq. (21) for wave heights.

also include the Rayleigh limits appropriate to linear waves, namely, Eqs. (20) and (21), in the same comparisons.

The results shown in Fig. 6 suggest that the wave-height exceedances observed compare with the predictions from Eq. (22) favorably, for the most part. It is noticed that at gauge 1, where the third-order modulations have not yet fully developed, waves are largely Gaussian. At all gauges, the observed distributions of wave crests are practically the same as those of trough amplitudes. This suggests that η_1 has a symmetrical statistical structure with respect to the mean water level, unlike η. The statistics of η observed at $x=45$ m (gauge 8) in the work of Cherneva *et al.*[21] and reproduced in Fig. 7 here show that in contrast with the results in Fig. 6(c) for η_1, η displays a significant crest-trough asymmetry. Evidently, the GC distributions describing wave crests and trough amplitudes also agree favorably with the observed empirical distributions, albeit not altogether impressively in all cases. Note in particular that as third-order quasiresonant

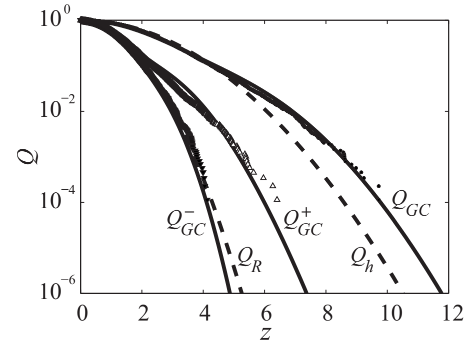

FIG. 7. Same as Fig. 6(c) except for η observed at $x=45$ m (gauge 8) from the wave maker, reproduced from the work of Cherneva *et al.* (Ref. 21). In this case, the theoretical distributions Q_{GC} for wave heights, Q_{GC}^{+} for wave crests, and Q_{GC}^{-} for trough amplitudes follow from the expressions given in Eqs. (8), (11), and (12) of the same reference.

interactions become significant, the observed distributions tend to deviate from the Rayleigh approximation for linear waves, also as predicted by the theoretical expressions.

VIII. CONCLUDING REMARKS

The present analysis and results on the properties of the theoretical NLS model and its invariants should provide additional insight into the nonlinear physics and statistics of mechanically generated waves. We have attempted to demonstrate this here with a detailed analysis of the free-wave component η_1 governed by the NLS equation in various comparisons with the empirical data gathered during the Marintek experiments. All this basically required the removal of the bound harmonics from the fully nonlinear time series η actually observed by way of a simple inversion procedure based on the assumption that the coupling between quasiresonant and nonresonant wave components can be expressed in a narrowband form, as in Eq. (1).

Notably, we observe that the spectra of both η and η_1 appear to be sensitive to viscous dissipation over the high-frequency range. The net effect is manifested as a decrease in the spectral bandwidth and a downshift of the mean frequency ω_m as waves propagate along the experimental basin. Further, we also observe a slight downshift of the spectral peak, plausibly due to modulations as reported in other similar experimental and numerical results.

One significant effect of quasiresonance modulations on the statistics of η_1 is a monotonic increase in the excess kurtosis along the basin. That in turn implies that wave crests and trough amplitudes are amplified symmetrically relative to the mean water level. As a result, their distributions progressively deviate from the Rayleigh form as waves propagate away from the wave maker. Such deviations appear to be reasonably well predicted by the third-order GC distributions considered here.

Our results suggest that the classical NLS equation is able to describe the statistical properties of unidirectional nonlinear waves reasonably well. Asymmetries of $O(\varepsilon)$ observed in the experiments and predicted by the higher order Dysthe or Zakharov models do not appear to noticeably affect the surface statistics considered here.

APPENDIX A

1. Derivation of η_1

We rewrite Eq. (1) as

$$\eta = \eta_1 + \frac{\beta}{2}(\eta_1^2 - \hat{\eta}_1^2) + \frac{3\beta^2}{8}(\eta_1^3 - 3\eta_1\hat{\eta}_1^2), \tag{A1}$$

where $\beta \ll 1$ and represents a parameter to be determined so that $\langle \eta_1^3 \rangle = 0$. From an inversion of the preceding expression, we obtain

$$\eta_1 = \eta - \frac{\beta}{2}(\eta^2 - \hat{\eta}^2) + \frac{\beta^2}{8}(\eta^3 - 3\eta\hat{\eta}^2) + O(\beta^3). \tag{A2}$$

The requirement that $\langle \eta_1^3 \rangle = 0$ leads to the expression

$$A_2\beta^2 - A_1\beta + A_0 = 0, \tag{A3}$$

correct to $O(\beta^2)$, where

$$A_0 = \langle \eta^3 \rangle, \quad A_1 = 3\frac{\langle \eta^4 \rangle - \langle \eta^2\hat{\eta}^2 \rangle}{2}, \tag{A4}$$

and

$$A_2 = \frac{9\langle \eta^5 \rangle - 21\langle \eta^3\hat{\eta}^2 \rangle + 6\langle \eta\hat{\eta}^4 \rangle}{8}. \tag{A5}$$

The physically meaningful solution of Eq. (A3) is

$$\beta = \frac{A_1 - \sqrt{A_1^2 - 4A_0A_2}}{2A_2}. \tag{A6}$$

APPENDIX B

1. Evaluation of the Integral J

The integrand of $J(\alpha)$ is not singular at $\alpha = 0$. So, from Eq. (16)

$$\frac{dJ}{d\alpha} = \frac{1}{(2\pi)^{3/2}} \times \int\int\int \exp\left(-\frac{z_1^2 + z_2^2 + z_3^2}{2}\right)\sin(\alpha Z)dz_1dz_2dz_3. \tag{B1}$$

Using complex notation, this expression can be rewritten as

$$\frac{dJ}{d\alpha} = \frac{1}{(2\pi)^{3/2}}\mathrm{Im} \times \int\int\int \exp\left(-\frac{z_1^2 + z_2^2 + z_3^2 - 2i\alpha Z}{2}\right)dz_1dz_2dz_3, \tag{B2}$$

or more simply,

$$\frac{dJ}{d\alpha} = \frac{1}{(2\pi)^{3/2}}\mathrm{Im}\int\int\int \exp\left(-\frac{\mathbf{u}^T\mathbf{\Omega}\mathbf{u}}{2}\right)d\mathbf{u}, \tag{B3}$$

where

$$\mathbf{\Omega} = \begin{bmatrix} 1 & -i\alpha & i\alpha \\ -i\alpha & 1 & i\alpha \\ i\alpha & i\alpha & 1-2i\alpha \end{bmatrix}, \quad \mathbf{u} = \begin{bmatrix} z_1 \\ z_2 \\ z_3 \end{bmatrix}. \tag{B4}$$

From the Gaussian identity

$$\frac{1}{(2\pi)^{3/2}\sqrt{|\mathbf{\Omega}^{-1}|}}\int\int\int \exp\left(-\frac{\mathbf{u}^T\mathbf{\Omega}\mathbf{u}}{2}\right)d\mathbf{u} = 1, \tag{B5}$$

it immediately follows that

$$\frac{dJ}{d\alpha} = \sqrt{|\mathbf{\Omega}^{-1}|} = \frac{1}{\sqrt{1 - 2i\alpha + 3\alpha^2}}. \tag{B6}$$

Integrating the preceding expression with $J(0) = 0$ will give

$$J(\alpha) = \mathrm{Im}\int_0^\alpha \frac{dx}{\sqrt{1 - 2ix + 3x^2}} = \frac{1}{\sqrt{3}}\left\{\frac{\pi}{6} - \mathrm{Im}\left[i\sin^{-1}\left(\frac{1 + 2i\alpha}{2}\right)\right]\right\}. \tag{B7}$$

ACKNOWLEDGMENTS

The second author has been supported by the Portuguese Foundation for Science and Technology with the Grant No. SFRH/BRD/30589/2006. The data analyzed here was obtained by the fourth author at Marintek, Trondheim in 1999 as a part of the project *Interactions between Waves and Currents*, partially funded by the European Union under Contract No. ERBFMGECT980135 for access to Large Scale Facilities.

[1]G. Lindgren, "Local maxima of Gaussian fields," Ark. Mat. **10**, 195 (1972).
[2]P. Boccotti, "Some new results on statistical properties of wind waves," Appl. Ocean Res. **5**, 134 (1983).
[3]P. Boccotti, *Wave Mechanics for Ocean Engineering* (Elsevier, New York, 2000).
[4]F. Fedele, "Rogue waves in oceanic turbulence," Physica D **237**, 2127 (2008).
[5]F. Fedele and M. A. Tayfun, "On nonlinear wave groups and crest statistics," J. Fluid Mech. **620**, 221 (2009).
[6]M. S. Longuet-Higgins, "The effect of nonlinearities on statistical distributions in the theory of sea waves," J. Fluid Mech. **17**, 459 (1963).
[7]M. A. Tayfun and F. Fedele, "Wave-height distributions and nonlinear effects," Ocean Eng. **34**, 1631 (2007).
[8]M. A. Tayfun, "Distributions of envelope and phase in wind waves," J. Phys. Oceanogr. **38**, 2784 (2008).
[9]V. E. Zakharov, "Stability of periodic waves of finite amplitude on the surface of deep fluid," J. Appl. Mech. Tech. Phys. **2**, 190 (1968) (English translation).
[10]V. E. Zakharov, "Statistical theory of gravity and capillary waves on the surface of a finite-depth fluid," Eur. J. Mech. B **18**, 327 (1999).
[11]M. Onorato, A. R. Osborne, M. Serio, and S. Bertone, "Freak waves in random oceanic sea states," Phys. Rev. Lett. **86**, 5831 (2001).
[12]C. Guedes Soares, Z. Cherneva, and E. Antao, "Characteristics of abnormal waves in North Sea storm sea states," Appl. Ocean Res. **25**, 337 (2003).
[13]C. Guedes Soares, Z. Cherneva, and E. Antao, "Abnormal waves during hurricane Camille," J. Geophys. Res. **109**, C08008 (2004).
[14]H. Socquet-Juglard, K. Dysthe, K. Trulsen, H. E. Krogstad, and J. D. Liu, "Probability distributions of surface gravity waves during spectral changes," J. Fluid Mech. **542**, 195 (2005).
[15]P. Petrova, Z. Cherneva, and C. Guedes Soares, "On the adequacy of second-order models to predict abnormal waves," Ocean Eng. **34**, 956 (2007).

[16] K. B. Dysthe, H. E. Krogstad, and P. Müller, "Oceanic rogue waves," Annu. Rev. Fluid Mech. **40**, 287 (2008).

[17] M. Onorato, A. R. Osborne, M. Serio, L. Cavaleri, C. Brandini, and C. T. Stansberg, "Extreme waves, modulational instability and second order theory: Wave flume experiments on irregular waves," Eur. J. Mech. B **25**, 586 (2006).

[18] M. Onorato, L. Cavaleri, S. Fouques, O. Gramstad, P. A. E. M. Janssen, J. Monbaliu, A. R. Osborne, C. Pakozdi, M. Serio, C. T. Stansberg, A. Toffoli, and K. Trulsen, "Statistical properties of mechanically generated surface gravity waves: A laboratory experiment in a three dimensional wave basin," J. Fluid Mech. **627**, 235 (2009).

[19] P. Petrova and C. Guedes Soares, "Maximum wave crest and height statistics of irregular and abnormal waves in an offshore basin," Appl. Ocean Res. **30**, 144 (2008).

[20] L. Shemer and A. Sergeeva, "An experimental study of spatial evolution of statistical parameters in a unidirectional narrow-banded random wavefield," J. Geophys. Res. **114**, C01015 (2009).

[21] Z. I. Cherneva, M. A. Tayfun, and C. Guedes Soares, "Statistics of nonlinear waves generated in an offshore wave basin," J. Geophys. Res. **114**, C08005 (2009).

[22] T. B. Benjamin and J. E. Feir, "The disintegration of wave trains in deep water: Part 1, theory," J. Fluid Mech. **27**, 417 (1967).

[23] P. A. E. M. Janssen, "Nonlinear four-wave interactions and freak waves," J. Phys. Oceanogr. **33**, 863 (2003).

[24] K. B. Dysthe, "Note on a modification to the nonlinear Schrödinger equation for application to deep water waves," Proc. R. Soc. London Ser. A **369**, 105 (1979).

[25] L. Shemer, E. Kit, and H. Jiao, "An experimental and numerical study of the spatial evolution of unidirectional nonlinear water-wave groups," Phys. Fluids **17**, 3380 (2002). AQ: #6

[26] C. C. Mei, *The Applied Dynamics of Ocean Surface Waves* (World Scientific, Singapore, 1989), pp. 1–760.

[27] E. Kit and L. Shemer, "On dissipation coefficients in a rectangular wave tank," Acta Mech. **77**, 171 (1989).

[28] L. Shemer, K. Goulitski, and E. Kit, "Evolution of wide-spectrum unidirectional wave groups in a tank: an experimental and numerical study," Eur. J. Mech. B/Fluids **26**, 193 (2007).

[29] M. J. Ablowitz and H. Segur, "On the evolution of packets of water," J. Fluid Mech. **92**, 691 (1979).

[30] A. Thyagaraja, "Recurrent motions in certain continuum dynamical systems," Phys. Fluids **22**, 2093 (1979).

[31] P. Petrova, C. Guedes Soares, and Z. Cherneva, "Influence of the third order nonlinearity on the distribution of wave height maxima in an offshore basin," Proceedings of the 27th International Conference on Offshore Mechanics and Arctic Engineering (OMAE2008), Estoril, Portugal, 15–20 June 2008, ASME Paper No. OMAE2008-58049.

[32] N. Mori and P. A. E. M. Janssen, "On kurtosis and occurrence probability of freak waves," J. Phys. Oceanogr. **36**, 1471 (2006).

[33] S. Y. Annenkov and V. I. Shrira, "Evolution of kurtosis for wind waves," Geophys. Res. Lett. **36**, L13603 (2009).

[34] M. A. Tayfun, "Distribution of large wave heights," J. Waterway, Port, Coastal Ocean Eng. **116**, 686 (1990).

AQ: #7

AUTHOR QUERIES — 028002PHF

#1 Au: Please verify change in working title.
#2 Au: Please verify changes in the affiliations and footnotes.
#3 Au: Please provide title for Appendix A.
#4 Au: Please provide title for Appendix B.
#5 Au: Please verify change in article title in Ref. 2.
#6 Au: Please verify that the volume should be ″14″ not ″17″ in Ref. 25.
#7 Au: Please verify journal title in Ref. 34.
#8 Au: Please verify changes in the Table.
#9 Au: Please verify changes in the Table.